Cell. Mol. Life Sci. 63 (2006) 285–300
1420-682X/06/030285-16
DOI 10.1007/s00018-005-5418-3
© Birkhäuser Verlag, Basel, 2006

Cellular and Molecular Life Sciences

Review

Recent results on hydrogen and hydration in biology studied by neutron macromolecular crystallography

N. Niimura [a, *], S. Arai [b], K. Kurihara [b], T. Chatake [c], I. Tanaka [d] and R. Bau [e]

[a] Institute of Applied Beam Science, Graduate School of Science and Engineering, Ibaraki University, 4-12-1 Naka-Narusawa, Hitachi, Ibaraki 316-8511 (Japan), Fax: +81 294 38 5254, e-mail: niimura@mx.ibaraki.ac.jp
[b] Neutron Science Research Center, Japan Atomic Energy Research Institute, 2-4 Shirakatashirane, Tokai, Ibaraki 319-1195 (Japan)
[c] Faculty of Pharmaceutical Sciences, Chiba Institute of Science, 3 Shiomi-cho, Choshi, Chiba 288-0025 (Japan)
[d] Department of Materials Science, the College of Engineering, Ibaraki University, 4-12-1 Naka-Narusawa, Hitachi, Ibaraki 316-8511 (Japan)
[e] Department of Chemistry, University of Southern California, Los Angeles, California 90089 (USA)

Received 12 September 2005; received after revision 19 October 2005; accepted 28 September 2005
Online First 2 January 2006

Abstract. Neutron diffraction provides an experimental method of directly locating hydrogen atoms in proteins, a technique complimentary to ultra-high-resolution [1, 2] X-ray diffraction. Three different types of neutron diffractometers for biological macromolecules have been constructed in Japan, France and the United States, and they have been used to determine the crystal structures of proteins up to resolution limits of 1.5–2.5 Å. Results relating to hydrogen positions and hydration patterns in proteins have been obtained from these studies. Examples include the geometrical details of hydrogen bonds, H/D exchange in proteins and oligonucleotides, the role of hydrogen atoms in enzymatic activity and thermostability, and the dynamical behavior of hydration structures, all of which have been extracted from these structural results and reviewed. Other techniques, such as the growth of large single crystals, the preparation of fully deuterated proteins, the use of cryogenic techniques, and a data base of hydrogen and hydration in proteins, will be described.

Key words. hydrogen; hydration; hydrogen bond; H/D exchange; protonation and deprotonation; neutron diffraction; protein crystallization.

Introduction

The three-dimensional structure determinations of biological macromolecules such as proteins and nucleic acids by X-ray crystallography have improved our understanding of many important life processes. In many cases, these results have clearly suggested that hydrogen atoms and water molecules around proteins and nucleic acids could play a crucial role in many physiological functions. However, since it is very hard to determine the positions of hydrogen atoms in protein molecules using X-rays alone, a detailed discussion of protonation and hydration sites often involves some guesswork. In contrast, it is well known that neutron diffraction provides an experimental method of directly locating hydrogen atoms, but unfortunately, to date, there are relatively few examples of biological systems studied by single-crystal neutron crystallography since the collection of a sufficient number of Bragg reflections is a time-consuming process. And, perhaps more important, the requirement of large single crystals (with volumes in the range of 1–10 mm^3) has been a serious limitation.

Breakthrough technical events in the neutron macromolecular field have been the development of the neutron imaging plate (NIP) [3–5], the adoption of Laue methods

* Corresponding author.

at reactor sources [6] and most recently the LANSCE time-of-flight electronic detector for neutron protein crystallography [8, 9]. Thus these three technical developments have allowed exploration of the main frontiers of the capability of neutron protein crystallography: namely, the time needed to measure data, the diffraction resolution reached and the molecular weight ceiling reachable.
Unfortunately, neutron protein crystallography still remains to this day a severely limited technique, but hopefully things will improve substantially in the coming future. The current development of 'next-generation' spallation neutron sources, such as the J-PARC (Japanese Proton Accelerator Research Complex) in Japan and the SNS (Spallation Neutron Source) in the USA, as well as new developments at existing sources i.e. LADI3 at the ILL and the proposed LMX++ at the ISIS TS2 (target station 2), will enable several more powerful protein crystallographic instruments to be installed. In these new spallation sources, a gain in neutron intensity of almost two orders of magnitude is expected. At that point, the use of neutron diffraction is expected to greatly expand the field of structural biology, and this topic will also be briefly discussed at the end of this article.
The general subject of neutron protein crystallography has been reviewed earlier by several authors [10–21]. Also of potential interest to readers are articles describing the synergy and complementarity between neutron diffraction and ultra-high-resolution X-ray diffraction [2, 21, 22]. In this paper, we will summarize selected results regarding hydrogen positions and hydration in proteins, obtained using the two BIX-type diffractometers in JAERI. Also included later in this review will be brief descriptions of recent results of the two other macromolecular neutron diffractometers that are being used today, LADI at ILL (Grenoble) [23] and PCS at LANSCE (Los Alamos) [24–26].

Instruments

BIX-type diffractometers (BIX-3, BIX-4)

After developing a novel practical neutron monochromator (a set of elastically bent perfect Si plates) and an original neutron detector (a gadolinium-doped neutron imaging plate), two BIX-type diffractometers (BIX-3 and BIX-4) dedicated for protein crystallography were constructed at JAERI, which were both effectively equipped with these two essential features [3–5]. The most characteristic and novel design of BIX-3 is the vertical arrangement of the main components of the diffractometer. This enables one to realize a compact design, and consequently a higher flux of neutrons is obtained because of the close proximity of the sample to the monochromator. Data are collected using a step-scan mode (typically 0.3°), with each exposure lasting between 30–60 min, and a total of 500–1000 of such frames are required for a typical data set [27]. A second machine, BIX-4, was constructed with a few additional improvements, but in principle it is nearly the same as BIX-3 [28].

Laue Diffractometer, LADI

The LADI diffractometer at the Institute Laue-Langevin (ILL) in Grenoble, France uses a Laue geometry and a broad spectral range to maximize the neutron flux on the sample [7, 23]. It effectively uses a very large number of reflections with a distribution of wavelengths, typically in the 3–4 Å range, which also substantially increases the crystal sample scattering efficiency to resolutions over 1.5 Å, selected via a Ni/Ti multilayer wavelength filter. Diffraction data are collected over a large solid angle by a cylindrical neutron imaging plate that completely surrounds the sample. Results from the LADI instrument have recently been reviewed by Meilleur et al. [20] and by Blakeley et al [21].

PCS Diffractometer at the LANSCE Pulsed Neutron Source

The PCS (Protein Crystallographic Station) diffractometer [24–26] located at the LANSCE neutron spallation source in Los Alamos National Laboratory (New Mexico, USA) is unique in that it is the first instrument designed to use a pulsed neutron source for macromolecular crystallography. Earlier single-crystal instruments that had been built for pulsed neutron beams include the SCD diffractometer at IPNS (Argonne, USA) [29] and the SXD diffractometer at ISIS (Didcot, UK) [30, 31], but those were optimized for much smaller unit cells associated with conventional (small-molecule) crystallography. The PCS instrument uses neutron pulses from a partially coupled moderator, and is equipped with a cylindrical ^{3}He gas detector of height 200 mm and an angular span of 120°. Results from the PCS instrument, which became operational in 2004, will be included in this review.

Comparison of existing instruments

As might be expected, each of the existing instruments has its advantages and disadvantages. It is probably fair to say that the PCS diffractometer at Los Alamos produces the data of the highest precision because of the low background level associated with its detector. But the disadvantage of that instrument is its low solid-angle coverage compared with the other two instruments, a feature which would require many more crystal settings and frames to collect a complete data set compared with LADI and the BIX machines. The LADI instrument located at the ILL is a faster diffractometer by a factor of 3–5 but the higher background level is a disadvantage. Finally, the BIX-3 and BIX-4 instruments at JAERI have produced the high-

est resolution (1.5 Å) neutron data sets thus far [32], but complete data collection times are relatively long (one or two months). Different variants of rubredoxin crystals have been collected on all three machines, and the resolution limits obtained are as follows: 1.5–1.6 Å at JAERI [32, 33], 2.1 Å at LANSCE [34] and 1.7 Å (at a temperature of 15 K) at LADI [20].

Crystal growth

Crystallization phase diagrams

One major disadvantage of neutron macromolecular crystallography is that large crystals are needed: currently, the volume of samples studied are normally larger than 1 mm^3. Usually such a large single crystal is difficult to grow. However, we have found that one rational way to find the proper conditions to grow large single crystals is to establish a detailed crystallization phase diagram. Figure 1a shows a typical protein crystallization phase diagram, where Cp and Cc are the protein and precipitant concentrations, respectively. The phase diagram is classified into three regions: unsaturated, meta-stable and supersaturated regions. Generally speaking, a large single crystal can be grown under supersaturated conditions close to the solubility boundary (the curved solid line in fig. 1a). Using a systematic way of evaluating the quality of crystals grown at various points in such a phase diagram, we have successfully grown large single crystals of three macromolecular samples: (i) cubic porcine insulin, (ii) dissimilatory sulfite reductase D and (iii) a DNA oligomer; all of which were successfully used in neutron protein data collection [35–37]. We have also applied a 'relative Wilson plot' method, involving quick X-ray data collections on selected crystalline samples, to evaluate the quality of crystals prior to neutron data collection [38].

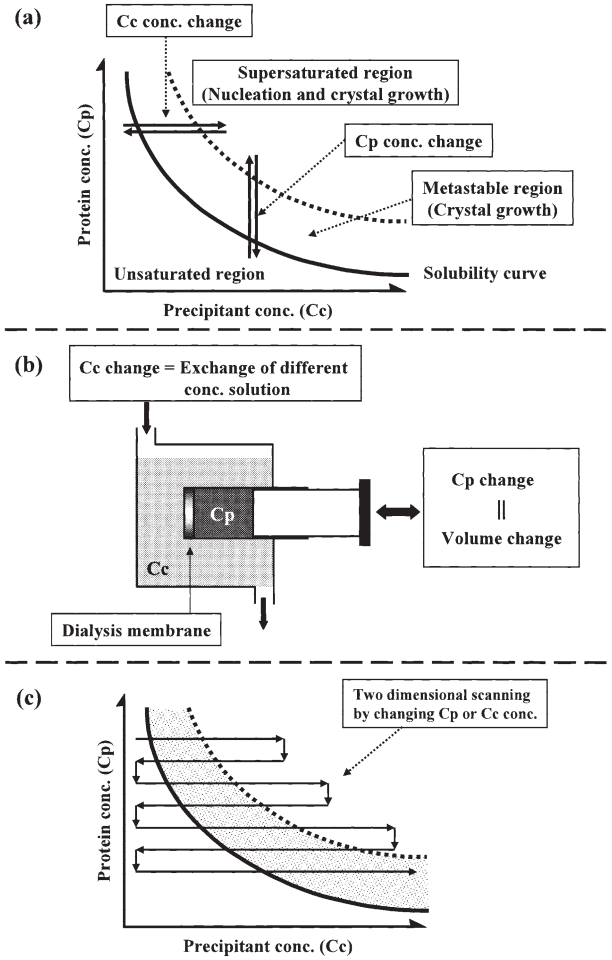

Figure 1. (*a*) A typical protein crystallization phase diagram. (*b*) Schematic drawing of an aparatus to control both Cp (protein concentration) and Cc (precipitant concentration) in a phase diagram. The novel feature here is that the volume of the protein solution can be accurately controlled. (*c*) One typical example of a pathway to determine the boundaries (solid and dotted curved lines) of a phase diagram.

Systematic control of protein solution volume in a crystallization experiment

In the normal dialysis method for growing crystals, the precipitant concentration is variable, but the protein concentration is kept constant. We have developed an apparatus in which the protein volume can be systematically varied (see fig. 1b). In this device, the protein solution (labelled 'Cp' in fig. 1b) is separated from the precipitant solution by a dialysis membrane. The important feature is that the volume of the protein solution can be accurately controlled by a syringe [Y. Ohnishi et al. unpublished]. In this new dialysis method, any combination of protein and precipitant concentrations can be surveyed in a systematic manner, for example via the pathway shown in figure 1c. Another significant advantage of our apparatus is that the total quantity of protein remains the same as the initial amount originally in the cell, and thus the entire phase diagram (fig. 1c) can in principle be mapped out with a very limited amount of sample material.

Other techniques for sample preparation

Deuteration

The current requirement of large single crystals of protein (over 1 mm^3) can be substantially reduced if the sample is totally deuterated. At present, most single-crystal neutron analyses are carried out with partially deuterated samples, in which a protein crystal is either soaked in a D_2O-containing solution after being formed, or the protein is dissolved in a D_2O-containing solution prior to crystallization. In either case, the procedure results in a sample in which D has replaced H in almost all of the O-H bonds, most of the N-H bonds but almost none of the

C-H bonds. The resulting partially deuterated crystal still retains a portion of the extremely large neutron incoherent scattering cross-section of hydrogen (~80 barns), which contributes to an undesirably large background to the diffraction data. In contrast, the corresponding incoherent scattering cross section for deuterium is much smaller (~2 barns), and complete deuteration would in principle offer as much as a 40-fold reduction in the background [39]. Indeed, this was accomplished not too long ago by Shu et al. [40], who reported the first neutron diffraction analysis of a fully deuterated protein, myoglobin. Complete deuteration can be accomplished by producing the target protein in a microbial expression system which has been adapted to growth in heavy water (D_2O) solutions and fed with deuterated carbon sources [39, 40]. Facilities for the preparation and crystallisation of fully deuterated proteins are currently available at the ILL-EMBL Deuteration Laboratory in Grenoble, France (http://whisky.ill.fr/YellowBook/deuteration). In addition, an important development is that similar deuteration facilities have also been recently established at Los Alamos [41] and are being planned for Oak Ridge [42]. A dramatic example of the beneficial effects of complete deuteration is the recent successful neutron analysis of a perdeuterated single crystal of aldose reductase having a volume of only 0.15 mm^3 [21]!

Neutron crystallography at cryogenic temperatures (~15 K)

The flash-freezing of protein crystals to liquid nitrogen temperatures (77 K) to minimize radiation-induced damage is now routine in X-ray crystallography [43]. Other advantages of this technique is that it often extends the diffraction limit to higher resolutions and produces a better-ordered structure. Unfortunately, it turns out that this procedure, while easily accomplished for the smaller crystals used in X-ray analysis, is much more difficult for the larger protein crystals used for neutron diffraction because larger crystals tend to crack more easily. Nevertheless, researchers at LADI have developed a procedure [20, 21] to cool and maintain large protein crystals at extremely low cryogenic temperatures (<15 K) and this instrument is now providing neutron diffraction data to high resolution (~1.5–2.5 Å). The basic idea of this technique is that the solvent must be rapidly flash-cooled to a vitreous glass in order to avoid ice formation that would disrupt or interfere with diffraction. In the LADI procedure, recently reviewed by Hansen [43a], the crystals are mounted in nylon loops and first flash-cooled to 77 K by plunging the sample directly into liquid nitrogen, and then in a second step the crystal is transferred, while still under liquid nitrogen, onto the cold head of a displex cryostat and further cooled to 15 K. Preliminary analysis of the refined 15 K structure of triclinic lysozyme, as compared with an earlier structure determination at 293 K [44], shows that the thermal motion of the protein is significantly reduced at the lower temperature, with a significant reduction in the overall protein B factor from 13.6 $Å^2$ to 8.6 $Å^2$ for the 293 K and 15 K structures, respectively [F. Meilleur et al., unpublished]. The LADI cryogenic procedure has also been applied successfully to crystals of rubredoxin (volume 1.4 mm^3) [20], aldose reductase (volume 0.15 mm^3) [21] and concanavalin A (volumes 1.6 and 5.6 mm^3) [45]. In the latter case it was even possible to identify full water molecules in the second and third hydration shells away from the protein surface, a feat which is usually unattainable via room-temperature neutron diffraction analysis.

Hydrogen and Hydration in Proteins Data Base

The results from neutron protein crystallography have been accumulating significantly in recent years, and we have realized that it is becoming increasingly important to deposit this information in a publicly accessible site so that the data can be retrieved more efficiently. We have created a 'Hydrogen and Hydration in Proteins' Data Base (HHDB) that catalogs all H atom positions in biological macromolecules and in hydration water molecules that have been determined thus far by neutron macromolecular crystallography [N. Niimura N. et al., unpublished]. This allows important structural information such as the geometry of H bonds to be abstracted and categorized for the first time in the field of structural biology.

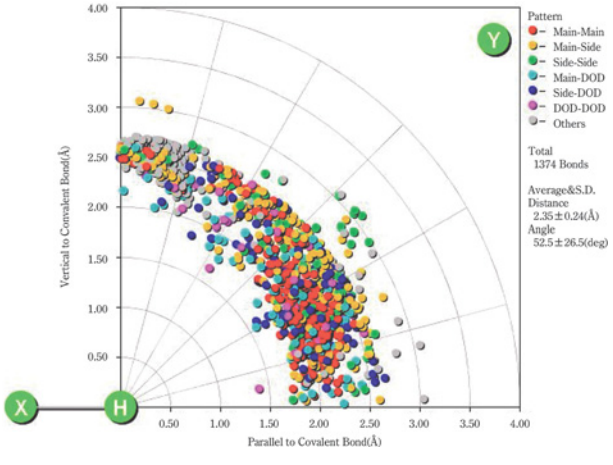

Figure 2. Schematic statistics of hydrogen bonds. Acceptor positions (Y) are searched and plotted in the first zone. In this example, H bond lengths are defined by X…Y values less than 2.7, 2.6 and 3.1 Å for the acceptor atoms N, O and S, respectively; and H bond angles are defined to be the supplement of 180 degrees. Note the very surprising result that in proteins there are very few acceptor atoms which form truly co-linear X-H–Y hydrogen bonds, in contrast to the situation in small inorganic and organic compounds in which linear H bonds are quite common (see text for a further discussion of this point).

The HHDB provides us with a graphic interface for visualizing all types of interactions involving H atoms, such as hydrogen bonds (defined by X–H...Y, where X is a hydrogen donor and Y is a hydrogen acceptor). For example, one type of plot (fig. 2) allows the user to visualize the distribution of the acceptor atoms (Y) as a function of H–Y distance and the supplementary X–H…Y angle (180° minus the actual angle). From these results, it is very surprising that in proteins there are very few acceptor atoms which form truly colinear X-H–Y hydrogen bonds, in contrast to the situation in small inorganic and organic compounds in which linear H bonds are quite common. The strengths of H bonds obtained in X-ray protein crystallography have often been assigned using the X–Y length as a criterion, but in our opinion, this assumption is very risky because this plot suggests that the usual argument that X-H–Y hydrogen bonds are approximately linear in proteins may not be valid.

The HHDB depository has been developed by cooperation between the Japan Science and Technology Agency (JST) and the Japan Atomic Energy Research Institute (JAERI) under a data base project funded by the JST. It is available via the website http://hhdb.tokai.jaeri.go.jp/HHDB/. From the HHDB, we have provided an Internet link to the Protein Data Bank (PDB), and the protein code and the nomenclature used in both databases are the same.

Results

Positions of hydrogen atoms in macromolecules

In JAERI, we have already analyzed the neutron structures of several proteins and two DNA oligomers: myoglobin [46], rubredoxin [32], a rubredoxin mutant [33], hen-egg-white lysozyme [6, 47], human lysozyme [K. Chiba-Kamosida, et al. unpublished], insulin [37], dissimilatory sulfite reductase D [36], and oligomers of B-DNA [48] and Z-DNA [49]. For example, consider the Asn21 residue of a rubredoxin variant [33], whose neutron and X-ray structures were determined at 1.6 and 1.5 Å resolutions, respectively. The amide side chain ($CONH_2$) of this residue is completely visible in the neutron map (fig. 3b), which also shows the NH_2 group being fully deuterated. In contrast, the two D atoms are completely missing in the X-ray map at a similar resolution (fig. 3a). In fact, the X-ray map shows a fairly symmetrical Y-shaped feature, meaning that it is very difficult in an X-ray analysis to distinguish the NH_2/ND_2 group from the O atom in an amide group because of the 'near-invisibility' of H atoms to X-rays (fig. 3a). In contrast, the neutron scattering length of a D atom is comparable to those of other non-hydrogen atoms, and thus the contour levels of an ND_2 group are about three times larger than those of an O atom (fig. 3b). In the rubredoxin mutant, 96% of H atoms have contours more negative than the –1.0 σ level, while all D atoms have positive contours higher than 1.5 σ, which means that practically all of the H and D atoms of the protein were directly observable at that resolution (1.6 Å). Even for neutron experiments carried out at medium resolution, most of the H/D atoms can be found. For example, in the neutron analysis of the protein DsrD, carried out at 2.7 Å resolution, about 60% of the H/D atoms of the molecule could be located [36].

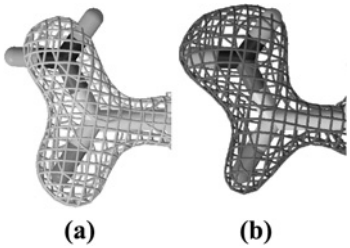

Figure 3. The $2|F_o|-|F_c|$ X-ray electron density map around the Asn21 residue of a mutant of rubredoxin (*a*), composed with the neutron density map of the corresponding residue (*b*). Note that in the X-ray map on the left, the contours themselves do not easily distinguish the ND_2 group from the O atom, while in the neutron map on the right the difference is very obvious.

Hydrogen Bonds

General comments

Hydrogen bonds clearly play important roles in countless biological processes. The strengths of hydrogen bonds are intermediate between those of covalent bonds and van der Waals forces: they are directional and form different types of networks under various conditions. Along with other investigators, Baker and Hubbard have extensively discussed H bonds in globular proteins, using hydrogen atom positions calculated using the atomic coordinates derived from high-resolution protein X-ray data [50]. It was pointed out that while most of the H positions in a protein can be reliably predicted (for example, those of C-H bonds), H positions could not be uniquely defined for most O-H, N-H and S-H bonds, such as those in Ser, Thr, Tyr, Lys, Cys, Asn, Gln, Asp, Glu, His and Arg side chains. And these are often the most interesting protons as far as chemical reactivity is concerned. In their conclusion, Baker and Hubbard stressed the necessity of high-resolution neutron diffraction studies. In this article we will discuss several examples in which this has been achieved through single-crystal neutron work, both from our labs and also those of other groups.

Bifurcated hydrogen bonds

In our studies of several small proteins, we have found that in most cases the hydrogen bonds between backbone C=O and N-H groups assume normal positions, such as that shown in figure 4 from an α-helix of myoglobin [46]. However, we have also found a few exceptions,

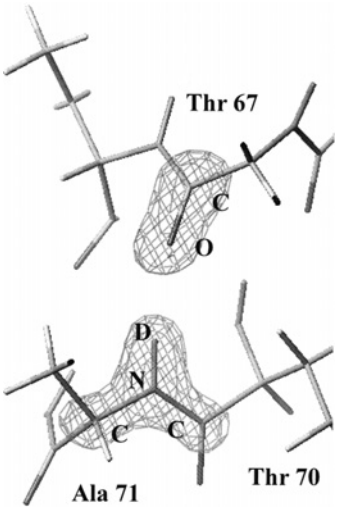

Figure 4. A typical hydrogen bond in an α-helix. $|F_o|-|F_c|$ omit nuclear density map from myoglobin.

such as bifurcated hydrogen bonds, one of which (also from myoglobin) is illustrated in figure 5. The occurrence of bifurcated hydrogen bonds in the α-helices of proteins had been proposed earlier, based on hydrogen atom positions calculated from the C, N and O coordinates from high-resolution X-ray data [51]. However, we feel that it is somewhat risky to discuss the detailed structure of hydrogen bonds based solely on those predictions, because often certain assumptions are made which may not be strictly true (such as the expectation that the CONH unit is perfectly planar). Indeed, we have found in our neutron studies that O-C-N-H torsion angles show deviations up to 15° from planarity, with a standard deviation of 6.3°. We suggest, therefore, that hydrogen bonds in α-helices cannot be described by a simple model, owing to complications such as bifurcated hydrogen bonds, which are often found near the ends of the helices.

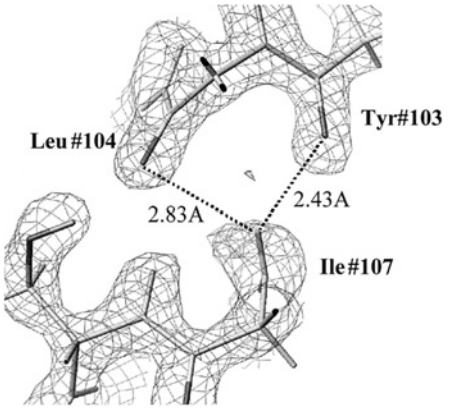

Figure 5. A typical example of a bifurcated hydrogen bond, as found in the neutron myoglobin structure.

H/D Exchange

Correlation of H/D exchange ratios with NMR results

As mentioned above, in most neutron experiments, in order to reduce background scattering from H atoms (which have a large incoherent scattering cross section), protein solutions are either subjected to H_2O/D_2O exchange prior to crystallization, or crystals are soaked in D_2O after crystallization from H_2O solution. This allows D atoms to be substituted for many of the H atoms, not only in the solvent water molecules, but also at sites containing 'exchangeable' hydrogen atoms (mostly H atoms of N-H and O-H bonds exposed to the solvent).

Nevertheless, some potentially exchangeable sites resist deuteration and remain hydrogenated. Figure 6a shows the region around some of the backbone N-H bonds of wild-type rubredoxin [32]: negative densities (red peaks) can be clearly seen at the H-containing sites, while positive densities (blue) are visible at the D-containing sites. Presumably, the N-H groups that have not been deuterated have resisted H/D exchange because of their poor solvent accessibility. Similar results have been observed in myoglobin [46] and in a rubredoxin mutant [33].

In the case of rubredoxin [32, 33], we have found that the H/D exchange ratio measurements from neutron data are roughly comparable with those from nuclear magnetic resonance (NMR) studies [52, 53]. The five red dots shown in Figure 6b (top) correspond to the five main-chain N-H groups that have not engaged in H/D exchange ratio (i.e. they have remained largely hydrogen). Compared with the distribution of B factors of the main chain atoms, it is seen that these five H/D atoms having small H/D exchange ratios also have small B factor values (fig. 6b, middle). The conclusion from these H/D exchange ratio measurements is roughly comparable with the results from NMR studies [52, 53] which show that there are two broad regions in the protein that display slow NMR H/D exchange behavior, one centered on the Cys5/Cys8 region and the other on Cys38/Cys41 (fig. 6b, bottom).

In fact, the set of backbone N-H bonds that show the slowest NMR exchange behavior include the five resistant N-H bonds that we have identified from our neutron data. Thus, there is very rough agreement between the NMR and neutron results, even though strictly speaking the two techniques are not directly comparable: NMR measures the dynamic behavior of a protein in solution, whereas neutron diffraction results reflect a static nature (i.e. a snapshot 'frozen in time').

Unusual examples of H/D exchange

In general, the H atoms of C-H bonds are not easily replaced by D atoms. However, two exceptional examples of H/D exchange were found in a protein structure and in an oligomeric DNA structure.

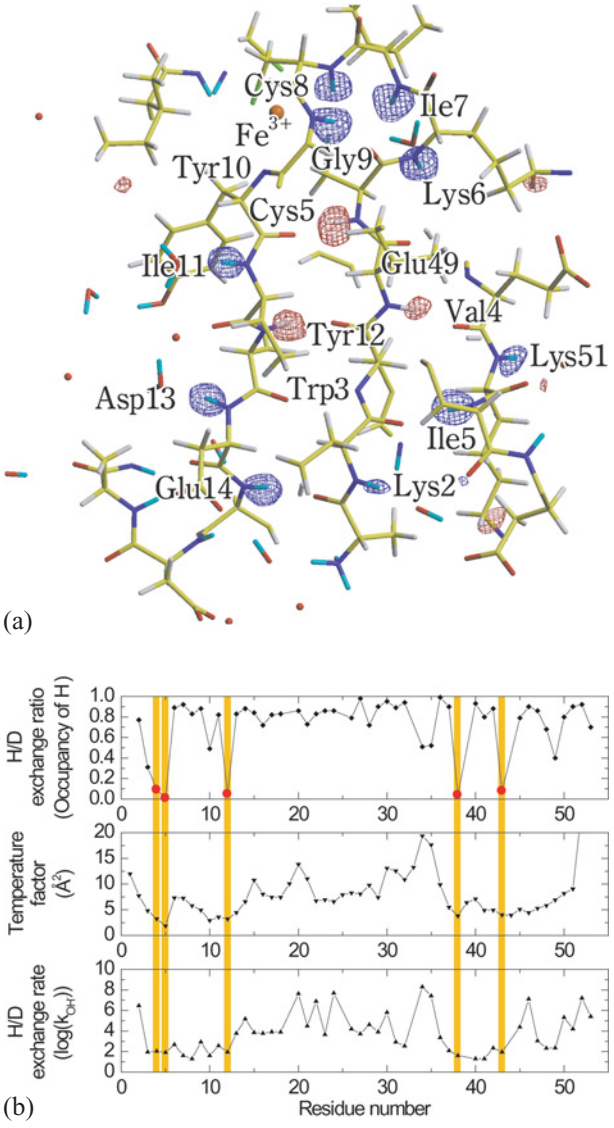

Figure 6. Hydrogen/deuterium exchange in rubredoxin. (*a*) The red (negative) and blue (positive) contours correspond to H and D atoms bonded to the main chain N atoms in this region. This plot shows three of the five H atoms that have not experienced significant H/D exchange. (*b*) (Right) The values of the neutron H/D exchange ratios (top) and B factors (middle) of main-chain H/D atoms. Also shown are the H/D exchange rates derived from the NMR results (bottom right plot; data taken from [52, 53]. The five red dots on the upper right-hand plot correspond to atoms that have resisted H/D exchange (i.e. atoms that are still mostly hydrogen), according to the neutron results.

Histidine

The first exception involves the C(ε_1)-H bond in the imidazole ring of histidine residues. This happens to be the most acidic C-H bond in amino acids [54], suggesting the possibility that it might participate in H/D exchange. We have recently confirmed via neutron diffraction that the C(ε_1)-H bond of histidine is in fact deuterated in myoglobin [46] and in insulin [37]. Figure 7 shows a neutron density map around His-97 in myoglobin. One clearly sees positive neutron density contours near C(ε_1), indicating that the C(ε_1)-H bond is now primarily a C-D bond. This particular C(ε_1)-H is pointing to a very disorderd solvent region and there is no special C-H–O hydrogen bonding. An occupancy refinement of this position yields the ratio 80% D/20% H [peak near H(ε_1) in fig. 7].

Guanine

Another example of H/D exchange involving a C-H bond was found in the guanine bases of d(CGCGCG)$_2$, a hexameric duplex form of Z-DNA [49]. The C_8-H_8 bond of guanine is similar to the C(ε_1)-H bond of histidine, in the sense that both are located between two nitrogen atoms of a five-membered ring. Previous proton-NMR studies had suggested that the C_8-H_8 bond can be deuterated in Z-DNA [55], and the present neutron analysis provides direct experimental evidence confirming this. Almost all the guanine bases in the crystal of d(CGCGCG)$_2$ showed evidence of a substantial amount of H/D exchange: an average of 75 % of the H_8 atoms in this duplex were found to have been replaced by D atoms. [49].

Protonation states of certain amino acid residues

Carboxylate groups of acidic residues

Neutron diffraction provides us with a detailed picture of protonation sites in a protein. Carboxylate groups (in Asp and Glu residues) and imidazole rings (in His residues) have pKa's in the range from 4 to 6, and their protonation and deprotonation equilibria may influence protein folding and function, as well as crystal packing between adjacent molecules. An example of the latter case was observed in the structure of dissimilatory sulfite reductase D (DsrD), whose crystal structure was determined at a

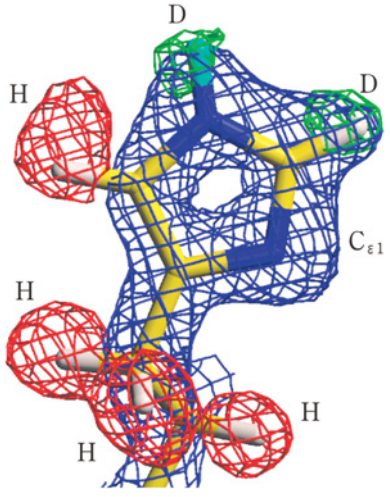

Figure 7. A neutron $|F_o|-|F_c|$ Fourier maps around His97 in myoglobin. Note the fact that the C(ε_1) – H(ε_1) bond of this imidazole ring has largely been deuterated.

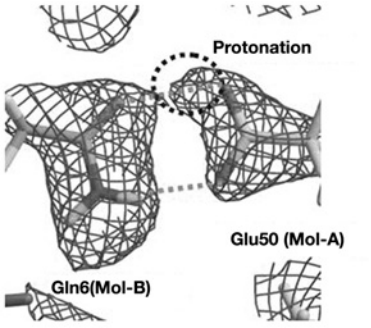

Figure 8. Interaction between the pseudo-two-fold symmetry axis relating two neighboring DsrD molecules. Broken lines are hydrogen bonds, while contours show positive neutron densities. Note the intermolecular hydrogen bonding between Gln6 of molecule B with Glu50 of molecule A. The upper H bond is between the C=O amide side chain of Gln6 and the carboxylate H–O of Glu50, while the lower hydrogen bond is from the N–H amide group of Gln6 to the unprotonated COOH oxygen of Glu50.

resolution of 2.7 Å [36]. In this crystal, two DsrD molecules form a dimer containing a non-crystallographic twofold rotation axis. A direct hydrogen bond was observed between Gln6 of one protein and Glu50 of its neighbor (fig. 8). This particular crystal form was grown at pD 5.5~6.5, while under less acidic conditions crystal growth tends to be slower. It can be speculated that protonation of the carboxylate group in Glu50 may play an important role in stabilizing intermolecular protein interactions in the crystal lattice.

Protonation state of the Nπ and Nτ atoms of histidine

Insulin is a polypeptide hormone that is intimately involved in the metabolism of glucose. The insulin monomer consists of two chains, a 21-residue A chain and a 30-residue B chain, linked by a pair of disulfide bonds. An understanding of the hydrogen bonding in insulin may be useful in understanding the physiological function of this hormone. X-ray diffraction techniques [56] showed earlier that the His-10 residue undergoes a conformational change as a function of pH, while His-5 does not show such a change, but the origin of this different behavior is not yet understood.

Neutron diffraction experiments of porcine insulin (crystallized at pH=9) were performed at room temperature [37]. Our neutron results show that, at this pH, both the Nπ and Nτ nitrogen atoms of His-10 are protonated (fig. 9a), while in the case of His-5 only the Nπ nitrogen atom is protonated (fig. 9b). These results explain the conformational change of His-10, and the absence of change of His-5, observed in an X-ray diffraction experiment [56]. The Nτ-*H* bond of His-10 forms a hydrogen bond to Tyr-A14, and it can be argued that an increase in pH causes the deprotonation of the Nτ nitrogen atom and the breakage of this His-10/Tyr-A14 hydrogen bond. On the other hand, in the case of the His-5 ring only the Nπ nitrogen atom is protonated at pH=9, and thus it does not show any pH-dependent structural changes. Thus, one can hypothesize that the protonation state of the Nπ and Nτ nitrogen atoms of imidazole can be the origin of this small structural change of insulin at different pH's.

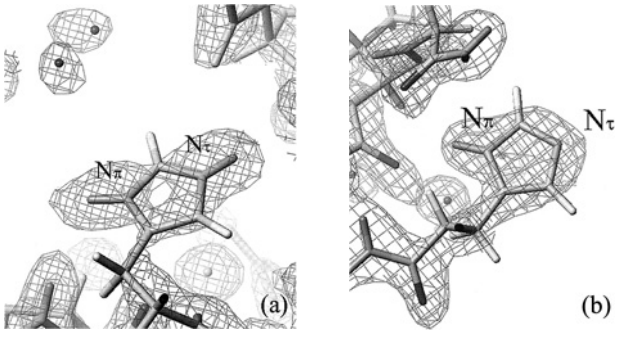

Figure 9. Protonation and deprotonation structures of histidines in porcine insulin observed by neutron diffraction. (*a*) For the 10th histidine residue, both the Nπ and Nτ nitrogen atoms are protonated in this diagram (however, at pH=10 the hydrogen atom bound to the Nτ nitrogen atom becomes deprotonated) (*b*) For the 5th histidine residue, the neutron data show that only the Nπ nitrogen atom is protonated.

Enzymatic activity

Lysozyme

The enzymatic activity of lysozyme, a saccharide-cleaving enzyme, is maximal at pH 5 and is less active at pH 7. It has been postulated that, at pH 5, the carboxyl group of Glu35 is protonated, and that it is this proton which is transferred to the oxygen atom of the bound substrate (an oligosaccharide) during the hydrolysis process. During the reaction, another acidic residue, Asp52, is postulated to remain in its dissociated (anionic) state [57]. To elucidate the role of hydrogen atoms in this reaction, neutron diffraction experiments of hen egg-white lysozyme have been carried out, using crystals which have been grown at different acidities: specifically, pD=4.9 on BIX [47] and pD=7.0 on LADI [6]. The 2|Fo|–|Fc| nuclear density maps around the carboxyl group of Glu35 are shown at pD 4.9 (fig. 10a) and at pD 7.0 (fig. 10b). At pD 4.9 the Fourier map shows a positive region (arrow in fig. 10a) extending beyond (i.e. attached to) the position of the O atom of the carboxyl group labeled E35 O(ε1), suggesting that this carboxyl oxygen atom (circled) is protonated at pD 4.9 (fig. 10a). On the other hand, at pD 7.0 it can be seen that this residue is deprotonated (circled atom in fig. 10b), and in its place there is a water molecule. The observation that the Glu35 catalytic site is deprotonated at pD 7.0 explains why lysozyme has significantly reduced activity at neutral conditions. Thus, our results suggest

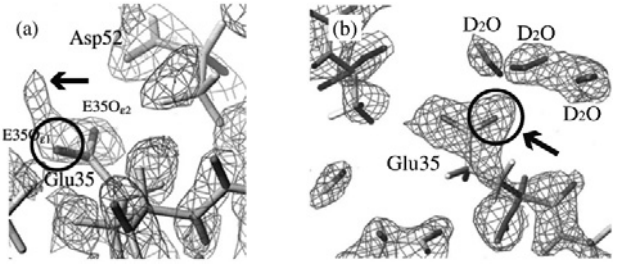

Figure 10. 2|Fo|–|Fc| nuclear density map around the carboxyl group of Glu35 of lysozyme at pD = 4.9 (*a*), and at pD = 7.0 (*b*). Note the pronounced 'finger' of nuclear density (see arrow) protruding upwards from atom E35O(ε1) on the left (pD = 4.9), and (*b*) the lack of such a feature on the carboxylate group on the right (pD = 7.0): that is, the oxygen atom has lost its proton. This suggests that residue E35 of lysozyme is in its protonated (deuterated) form under more active (acidic) conditions. [Note: in both plots, atom E35O(ε1) is circled].

that Glu35 is the site of the enzymatically active proton that is subsequently transferred to the oxygen atom of the carbohydrate substrate during the hydrolysis process. Incidentally, our results at the less acidic pH (7.0) [6] are consistent with the conclusions of an earlier neutron investigation, as described in a paper by Mason and coworkers many years ago [58].

Endothiapepsin

Endothiapepsin is a member of a class of important protein-cleaving enzymes, the aspartate proteinase family (of which renin and HIV protease are other examples). In a recently-completed study using LADI by Cooper, Myles and co-workers [59, 60] on fungal endothiapepsin complexed with a transition-state analog, it was established that the two key catalytic aspartate residues situated at the active site are in different protonation states in the active enzyme. From the 2.1 Å neutron study carried out with LADI at ILL, it was conclusively shown that Asp-215 is in the neutral (protonated) state, while Asp-32 is not (fig. 11a), thereby supporting a proposed mechanism in which a key step is the involvement of a tetrahedral intermediate stabilized by a negatively charged Asp-32 and a neutral Asp-215 residue (see intermediate states labeled '2' and '3' in fig. 11b).

Xylose isomerase

In one of the first papers produced from data collected at the PCS diffractometer in Los Alamos [24–26], Hanson and co-workers reported [61] preliminary work on the enzyme xylose isomerase at high resolution (ca. 2.0 Å). Bacterial D-xylose Isomerase (XI) is a protein of molecular weight of ~160 kDa, crystallizing in an orthorhombic space group, with unit cell dimensions ca. 94×99 ×103 Å. Crystals with size ranges of 1.5–3.5 mm on a side were grown, and about 182,000 reflections could be collected over a total time period of about 3 weeks. XI not only acts upon its normal substrate D-xylose, but is also an important enzyme industrially because it is used to convert D-glucose to D-fructose. A key recent finding [20, 21] is that residue His-53 in XI appears to be protonated at both nitrogen positions, in accordance with a proposed mechanism [62] in which His-53 is postulated to donate its HD2 proton to the sugar oxygen O5 to promote the ring opening. Currently, a second data set is being collected to higher resolution and accuracy, with a different metal at the catalytic site (cobalt instead of manganese) G. J. Bunick and J. P. Glusker, unpublished; Langan P., private communication].

Aldose reductase

The work on aldose reductase (an enzyme of paramount importance in diabetes) [I. Hazemann et al., unpublished] deserves special mention, since even an ultra-high-resolution X-ray data set (0.66 Å) was unable to supply information on the catalytically active hydrogen atoms in the active site of this important enzyme [63]. A neutron data set, collected to 2.2 Å resolution at LADI on a fully deuterated crystal just 0.15 mm^3 in volume, has succeeded in providing unique information about the mechanism of action of this enzyme [20, 21]. This work represents an outstanding example of the importance of complete deuteration in future applications of macromolecular neutron crystallography. And as in the case of concanavalin A [22, 45], aldose reductase has been the subject of a careful comparison between neutron diffraction [21] and ultra-high-resolution X-ray results [63].

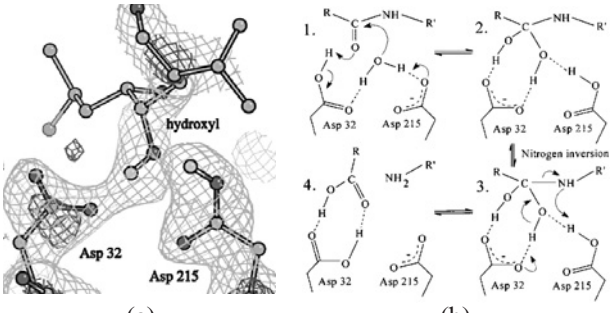

Figure 11. (*a*) Neutron difference map showing the active site region of endothiapepsin (an aspartate protease) complexed with a transition state analogue. In this 2.1 Å-resolution neutron study by Cooper, Myles and co-workers, Asp-32 was found to be in its deprotonated state, while Asp-215 is protonated. (Reproduced with permission from [60]). (*b*) The catalytic mechanism proposed for aspartate proteases (see discussion in [60]), in which a water molecule tightly bound to the key aspartate residues in the active site of the enzyme is involved in a nucleophilic attack on the carbonyl group of the peptide bond to be cleaved. Note the protonated state of Asp-32 and Asp-215 in intermediate stages (2) and (3), which is consistent with the neutron results [fig. 11a] (reproduced with permission from [Ref. 60]).

Cytochrome P450cam

Cytochrome P450's are ubiquitous heme-containing enzymes responsible for a large number of biological oxidations. They catalyze the two-electron oxidations of a wide variety of hydrocarbons from molecular O_2, but the manner in which this is accomplished (e.g. the proton-delivering pathway and the nature of the H bonding pattern near the active site) is not fully understood. Neutron data sets on hydrogenated and deuterated samples of cytochrome P450cam (also known as camphor monooxygenase) have been collected up to a resolution of 1.7 Å at LADI [64] (F. Meilleur F. et al., unpublished], and the structural analysis is currently in progress.

Amicyanin

Blue copper proteins are abundantly found in nature as long-range electron transfer agents. In these metalloproteins, the copper redox site is coordinated by two imidazole rings from His residues, one Cys group and one Met residue in a highly distorted N_2S_2 tetrahedral environment. One of these intensely blue proteins, amicyanin (isolated from the bacterium *paracoccus denitrificus*) is currently under neutron study [65]. When amicyanin is reduced, one of the copper ligands, His-95, rotates by 180° relative to its position in the oxidized state and actually moves away from the copper coordination sphere. It has been hypothesized that the reason for this remarkable disengagement is that His-95 is doubly protonated in the reduced state and singly protonated in its oxidation state [66]. A large dark blue crystal (2.0 ×1.3×1.0 mm) was grown over a period of several months via a repeated macroseeding technique, and neutron diffraction data were collected at the PCS (Los Alamos) over a 3-week period up to a resolution of 1.9 Å [65]. The structural analysis is currently in progress.

Dihydrofolate Reductase (DHFR)

Dihydrofolate Reductase (DHFR) is an important enzyme involved in the regeneration of tetrahydrofolate (THF), which in turn is a critically important metabolite involved in a large number of single-carbon transfer reactions, for example the conversion of deoxyuridine to thymidine, leading ultimately (in that case) to the production of the DNA base thymine. A key question in the structure of DHFR concerns the role of an important residue in the active site of the enzyme, Asp-27, whose protonation state under various conditions is still uncertain. There is also a water molecule at the active site whose precise function is probably critical but is not fully understood. Neutron diffraction data on single crystals of dihydrofolate reductase have been collected both at ILL [B. C. Bennett et al., unpublished] as well as at LANSCE [C. G. Dealwis and B. C. Bennett, unpublished; Langan P., private communication] in an attempt to elucidate the mechanism of this important enzyme.

Protocatechuate 3,4-Dioxygenase (3,4-PCD)

This is a metalloenzyme involving a trigonal bipyramidal iron atom at its active site. The five ligands around iron include two nitrogens from His, two oxygens from Tyr and a water molecule [67]. The protonation states of the ligands around the iron atom during the reaction cycle remains unknown. Neutron diffraction data have recently been collected at the PCS instrument at Los Alamos up to a resolution of 2.5 Å [68]. The remarkable feat in this case is the fact that this protein represents the largest biological molecule ever studied at moderately high resolution using single-crystal neutron techniques. The 3,4-PCD aggregate is a dodecamer of 587 kDa, with unit cell dimensions of 223×127×134 Å! The quality of the data is currently being evaluated, and this structural analysis, if successful, will certainly provide a technical basis for future neutron studies of other large biological macromolecules.

Other published structures

Other published structures include those of the Trp repressor, a DNA-binding protein [69] (data collected at the LADI diffractometer at ILL), and the W3Y mutant of rubredoxin from *Pyrococcus furiosus* [34] (data collected at the PCS diffractometer at LANSCE). Owing to lack of space, it will not be possible to discuss these structure determinations in this review, and the reader is referred to the original publications for more details.

Water molecules of hydration

Classification

We have categorized observed water molecules into the following classes based on their appearance in Fourier maps [18, 19, 70]: (i) triangular shape, (ii) ellipsoidal stick shape and (iii) spherical shape, and in some cases molecules of the second category (ellipsoidal stick shapes) can be further subclassified as either (iia) short and (iib) long. We found that this classification conveniently reflects the degree of disorder and/or dynamic behavior of a water molecule. Full details are given in the original publications [18, 33, 70], but the essential conclusions are summarized in figure 12. A triangular shape indicates a completely ordered water molecule, with all three atoms located (fig. 12a), while a short ellipsoidal shape indicates that the O-D bond is visible while the second D atom is disordered (fig. 12b). A long ellipsoidal contour (which is rarely observed) shows two ordered D atoms with the central O disordered (fig. 12c), while the very common spherical shape (fig. 12d) corresponds to a completely disordered water molecule. In an X-ray map, all four types of water molecules would appear simply as spherical peaks, and hence it is apparent that neutron maps are much more informative about hydration struc-

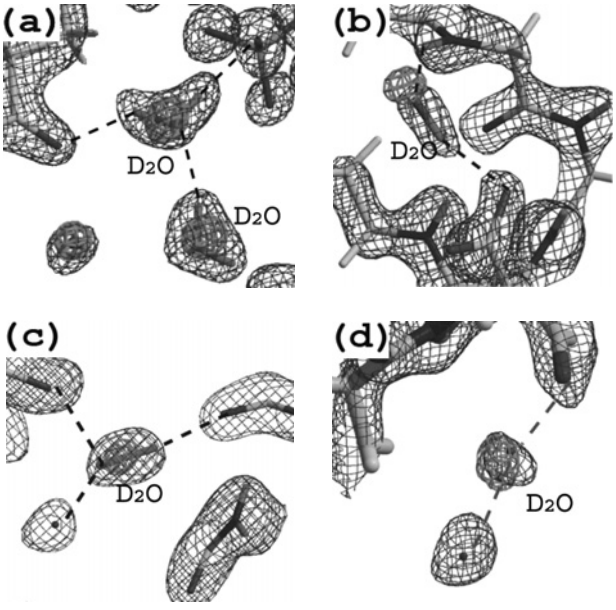

Figure 12. $2|F_o|-|F_c|$ neutron Fourier maps of water molecules of hydration for a rubredoxin mutant and and a myoglobin. Examples shown are peaks having (*a*) a triangular shape, (b) a short ellipsoidal shape, (*c*) a long ellipsoidal shape and (*d*) a spherical shape. In these figures, the central peak (inner contours) embedded in the middle of each water contour corresponds to the oxygen atom position derived from X-ray data. Note that, from the outer contours, in (*a*) all atoms of the central D_2O molecule are visible, whereas in the other diagrams only some of the solvent atoms are visible in the neutron maps: O and D in (*b*); two D in (*c*); and only O in (*d*).

ture, especially concerning the water molecules near the surface of a protein, which are much more likely to be ordered.

oligomeric DNA duplexes

It has long been suspected that the structure and function of a DNA duplex can be strongly dependent on its degree of hydration. In order to investigate the hydration structure of small oligomeric segments of duplex B-DNA [48] and Z-DNA [49], neutron diffraction studies have been carried out on such samples using the BIX-3 and BIX-4 single-crystal diffractometers at JAERI.

The B-DNA decamer d(CCATTAATGG)$_2$

Previous X-ray studies of oligomeric B-DNA have shown that the hydration pattern in the minor groove, especially at A•T-tract sequences, is relatively well-ordered [71–73]. In those X-ray studies, the observed hydration structure was inferred from the network of oxygen atoms of the water molecules. Goodsell et al. have described the 2.3 Å resolution X-ray structure of the d(CCATTAATGG)$_2$ duplex and have discussed the implications of B-DNA bending at T-A sites [74]. In that paper the hydration structure in the minor groove of d(CCATTAATGG)$_2$ was also described, in which hydrogen bonds from water to DNA were assumed to exist for all defined O...O distances less than 3.5 Å [74]. From our 3.0 Å neutron study [48], the observed water network in the minor groove of d(CCATTAATGG)$_2$, is shown in figure 13. In many cases, the orientations of water molecules can be deduced from the positions of the deuterium atoms, and it was observed that the DNA-water interactions are actually quite complicated: the complexity of the hydration pattern in the minor groove is derived from the extraordinary variety of orientations of the water molecules (fig. 13). This result has already been discussed in detail [48].

The Z-DNA hexamer d(CGCGCG)$_2$

Z-DNA has a zigzag arrangement of the backbone atoms in an unusual left-handed helical arrangement. Originally viewed as a structural oddity, Z-DNA is now believed to play a significant biological role [75]. The Z-DNA hexameric duplex d(CGCGCG)$_2$ was investigated by high resolution X-ray crystallographic analysis (0.6–1.0 Å), and the positions of water molecules in the hydration shell were determined precisely [76–79]. Nevertheless, even at this high resolution the orientational information of water molecules could not be obtained from the X-ray data. We have obtained the 1.8 Å resolution structure of this duplex by neutron crystallographic analysis [49], which showed 44 water molecules, of which 29 of them possessed a triangular (ordered) shape. The remaining 15 water molecules had a simple spherical (disordered) shape. An inter-

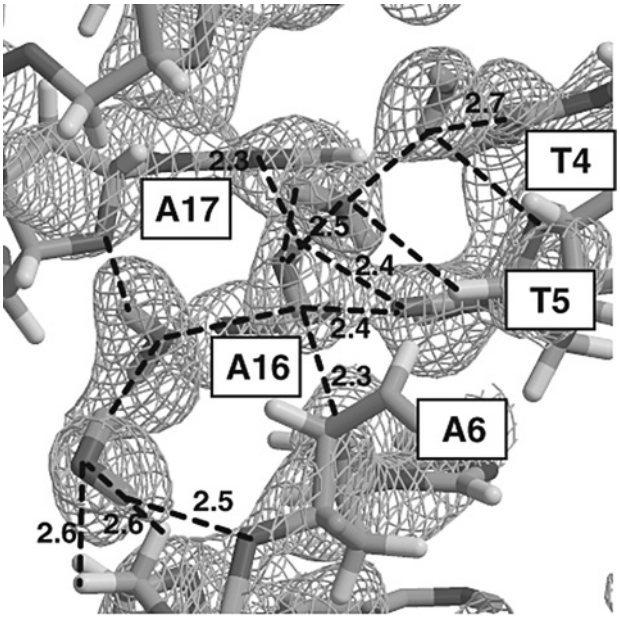

Figure 13. $2|F_o|-|F_c|$ neutron Fourier map (3.0 σ level) in the minor groove of the B-DNA decamer d(CCATTAATGG)$_2$. The bases Thy4, Thy5, Ade6, Ade16 and Ade17 are labelled in this figure. Broken lines indicate the hydrogen bonds. Note that a complicated (but ordered) water network has been observed tightly associated with the minor groove. In contrast, many of the water molecules in the major groove (not shown here) are disordered.

esting relationship was found between the orientational disorder of the water molecules and their locations: almost all water molecules in the minor groove were well-ordered in the crystal, whereas about half of the water molecules in the major groove were rotationally disordered. This type of disorder was also observed in the neutron crystal structure of B-DNA discussed in the previous section [48], which also showed the water in the minor groove to be more highly structured than that in the major groove. The complicated hydrogen-bonding networks in the hydration shells of $d(CGCGCG)_2$ have been discussed in detail [49].

Water structure in Concanavalin A

Concanavalin A (ConA) has been studied several times by the Helliwell group in collaboration with ILL/LADI scientists [7, 22, 45, 80, 81], primarily for the purpose of methods development, as well as to illustrate the complementarity between high-resolution X-ray results and medium-resolution neutron results [2, 7]. Con A is a saccharide-binding protein containing calcium and manganese, and it was originally investigated by Habash, Wilkinson, Helliwell, Lehmann and co-workers in 1997 as one of the first examples of the use of the LADI diffractometer [80]. A later report extended its resolution from 2.75 to 2.4 Å, which enabled some of the D_2O molecules in the structure to be observed (for the first time) as well-defined triangular-shaped contours [22]. In particular, the D_2O ligands of the Ca and Mn atoms were clearly visible in fine detail, as well as the water molecules that were found in the carbohydrate-binding cavity that is normally filled with the saccharide substrate in the complexed form of the protein. In the most recent study of this protein, also carried out to 2.5 Å resolution but now at the extremely low temperature of 15 K, full D_2O waters with complete contours could be observed even up to the second and third hydration shells [45]. Not only was this the first demonstration that large protein crystals (5.6 and 1.8 mm^3, respectively) could be frozen successfully, but another interesting feature of that study was a careful analysis of the quality of the large crystal used in the cryogenic work after neutron data collection. It was observed that the portion of the crystal first exposed to low temperature (as it was plunged into liquid nitrogen) suffered the worst damage due to thermal shock, but that as one moved away from that point of contact towards the other regions of the large sample, crystal quality improved. Finally, a comparison of water contours (Fourier maps) between (i) room temperature neutron data; (ii) 15 K neutron data and (iii) 110 K X-ray data shows some interesting features [45]: for example, even though the room temperature neutron data set [22] and the 15 K neutron data set were collected at about the same resolution level (2.5 Å), the five water molecules at the saccharide-binding site were poorly resolved at room temperature (i.e. they appeared as a single merged peak) [22], whereas at 15 K the solvent molecules could in fact be observed as individual peaks [45]. Incidentally, the times required for these data collections were (approximately) 10 days [80], 11 days [22] and 34 days [45]. The authors also attempted to collect data on concanavalin complexed to a substrate analog (methyl-α-D-glucopyranoside) of 50 kDa in the crystal asymmetric unit, but the diffraction resolution was only ~3.5 Å due to the large unit cell volume even for a long exposure. Unfortunately), technical problems with the reactor interrupted the neutron beam time and prevented completion of the 3.5 Å data set. [81].

Thermostability

Structural results from neutron diffraction can also provide some indirect information regarding protein thermostability. We have investigated two forms of the unusually stable rubredoxin from a hyperthermophilic archeobacterium (*Pyrococcus furiosus*), a protein which can survive almost 2 days of heating at 90 °C without appreciable denaturation. These two neutron diffraction analyses were solved at 1.5 and 1.6 Å resolution, respectively [32, 33]. An interesting observation was found involving the N-terminus itself, which participates in a tight 'arc' of H bonds involving several amino acids (fig. 14). Intriguingly, one of the key residues in this arc is Glu-14, which is not found in rubredoxins from mesophilic (i.e. room temperature) microorganisms. One can speculate that perhaps this 'tying down' of the N-terminus might be one of the many factors of that could contribute to the extraordinary thermostability of this protein.

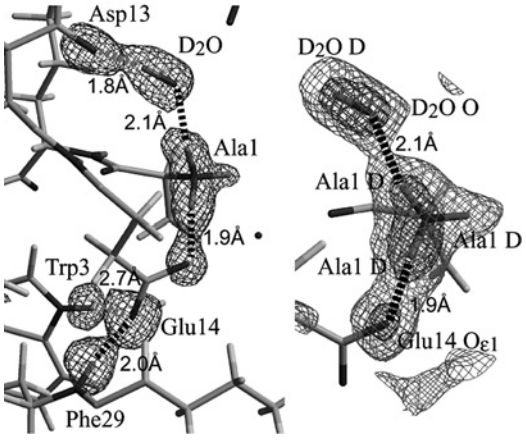

Figure 14. (Left): $|F_o|-|F_c|$ omit map showing the 'arc' of hydrogen bonds around the N-terminal region of wild-type rubredoxin. Contouring level is 3.0 σ, and hydrogen bonds are shown as dotted lines. (Right): Expanded view of the terminal ND_3^+ group (inside contours, at 2.0 σ; outside contours, at 4.0 σ), showing all three D atoms of this group to be resolved.

Future prospects

Challenging Structures (crystals with large unit cells)
Attempts have been made at ILL to collect neutron data on the methyl α-D-glucoside complex of con A (space group cubic, $I2_13$, a=167 Å) [81] and from the large iron storage protein complex ferritin (space group cubic, F432, a=183 Å). These efforts have demonstrated the potential to collect useful data to medium resolutions (3.5 Å) [81], but the recent work on protocatechuate 3,4-dioxygenase from the Los Alamos group (space group monoclinic, C2, unit cell 223×127×134 Å) [68] suggests that data collection on crystals having large unit cells may become more feasible in the near future than originally thought. However, it should be pointed out that these large unit cells are all centered, and that the equivalent primitive unit cell dimensions, and the spot-to-spot separations in the three cases, are rather similar. Ahmed et al. have outlined new ideas to reach up to spherical virus neutron crystallography; these ideas involve using the benefit of high non-crystallographic symmetry to relax the resolution limit required to see deuterium atoms and use of colder neutrons (λ=~6 Å) to increase the sample scattering efficiency [82].

'Next-generation' spallation neutron sources
An exciting new development currently under way is the construction of high-intensity, state-of-the-art pulsed neutron facilities. These are the Spallation Neutron Source (SNS) at Oak Ridge, Tennessee in the United States and the Japan Proton Accelerator Research Complex (J-PARC) in Ibaraki prefecture in Japan. Both SNS and J-PARC promise to deliver neutron intensities that are at least an order of magnitude (or more) higher than those at existing sources: traditional nuclear reactors such as those at ILL in Grenoble (France) and JRR-3 in JAERI (Japan), as well as existing pulsed (spallation) neutron sources such IPNS in Argonne (USA), ISIS at Didcot (England) and LANSCE at Los Alamos (USA).
At both new high-intensity spallation sources, diffractometers for macromolecular crystallography are either being built or planned. At J-PARC, construction of the so-called BIX-P1 instrument has already been in progress since 2004; while at the SNS a corresponding instrument, to be called MaNDi (Macromolecular Neutron Diffractometer) is being proposed. The instruments will differ somewhat in the type of moderator used (this is the material situated between the neutron target source and the sample crystal; its choice determines the intensities and wavelength distribution of the neutrons used in the diffraction experiment). BIX-P1 will be using neutrons from a coupled moderator, which has a higher intensity but a wider wavelength range; while MaNDi is proposed to use a decoupled moderator, which is less intense but has a sharper distribution. One reason for this difference is that J-PARC has a lower pulsing frequency (25 Hz) than SNS (60 Hz): overlap between pulses that are separately more widely in time is therefore less serious of a problem at J-PARC than the closely spaced pulses at SNS.
Regardless of these technical differences, the implications of the development of SNS and J-PARC on macromolecular research are obvious: if intensities can be increased by an order of magnitude or two, then in principle it will be possible to study crystals that are correspondingly smaller in volume. The consequences of this development will be enormous. A dramatic decrease in crystal size will have an absolutely dramatic effect on the usefulness of single-crystal neutron diffraction in the field of structural biology. It is hoped that both instruments will become operational around the period 2009–2010.

Conclusions

1) Activity in the single-crystal neutron analysis of proteins has increased dramatically in recent years: at JAERI (Japan), BIX type diffractometers equipped with neutron imaging plates (NIPs) and at ILL (France), the LADI diffractometer has been successfully used to acquire high-resolution neutron diffraction data for the location of hydrogen atoms and molecules of hydration in proteins and oligomeric nucleic acids. The PCS instrument at Los Alamos, using a pulsed neutron source, has also begun producing a steady stream of results.
2) We have found that crystallization phase diagrams are very helpful for systematically determining the optimal conditions for growing large single crystals for neutron biomacromolecular crystallography. A new method for determining these phase diagrams, involving the careful control of protein solution volumes via a syringe and a dialysis membrane, is being developed. In addition, a rational way to assess the quality of protein crystals, based on the analysis of relative Wilson plots, has been proposed.
3) Parallel improvements in modern molecular biology now allow fully perdeuterated protein samples to be produced for neutron scattering that essentially eradicate the large – and ultimately limiting – hydrogen incoherent scattering background that has hampered such studies in the past. This also substantially increases the protein crystal scattering efficiency, as deuterium scatters strongly and there are many deuterium atoms in a fully perdeuterated protein. High-quality neutron data can now be collected to near atomic resolution (~2.0 Å) for proteins of up to ~50 kDa molecular weight using crystals of volume ~0.1 mm^3.
4) The ability to flash-cool and collect high-resolution neutron data from protein crystals at cryogenic temperatures have been implemented

5) A Hydrogen and Hydration in Proteins Data Base (HHDB) that catalogs hydrogen atoms and hydration water molecules in proteins, as determined by neutron protein crystallography, has been created and is already publicly available.
6) Certain structural features related to H atoms have been determined. (i) Since almost all the protein H atom positions can be identified experimentally, the geometrical details of certain types of H bonds can be visualized; (ii) since the neutron scattering process distinguishes deuterium from hydrogen, information regarding the H/D exchange behavior of proteins can be obtained, and in some cases it has been found to be comparable to the results obtained from NMR spectroscopy; and (iii) perhaps most important, as far as mechanistic implications are concerned, the identification of protonation and deprotonation states of certain important amino acid residues can be carried out.
7) The hydration structure around proteins and the hydration networks around DNA oligomers have been successfully characterized in several exemplary cases.
8) Future protein crystallographic instruments, such as BIX-P1 and the proposed ManDi diffractometer, at 'next-generation' high-intensity spallation (pulsed) neutron sources, promise gains in performance that will further extend the size and complexity of samples (and, more important, reduce crystal sizes) that can be studied by neutron crystallography. Also, there are new developments at existing neutron sources to enhance their neutron protein crystallography instrumentation, i.e. LADI-3 at the ILL. And for target station 2 (TS2) at ISIS, the new proposed initiative of a Large Molecule Neutron Diffractometer (LMX++) will enable new types of neutron protein crystallography experiments for European researchers, too.

Acknowledgments. Most of this research was supported in part by an Organized Research Combination System (ORCS) grant from the Ministry of Education, Culture, Sports, Science and Technology of Japan. We are grateful to the those scientists involved in that effort, including those who took part in several international workshops hosted in JAPAN, and also to Profs. J. R. Helliwell and E. Westhof for their work on the ORCS Advisory Committee over a 5-year period. We also thank the U.S. National Science Foundation (grant CHE-98–16294 to R.B.) for partial support of this work, and we are grateful to Dr. D. Myles and Dr. P. Langan for providing the results obtained in ILL and LANSCE (respectively) in advance.

1 Petrova T. and Podjarny A. D. (2004) Protein crystallography at subatomic resolution. Rep. Prog. Phys. **67:** 1565–1605
2 Blakeley M. P., Cianci M., Helliwell J. R. and Rizkallah P. J. (2004) Synchrotron and neutron techniques in biological crystallography. Chem. Soc. Rev. **33:** 548–557
3 Niimura N., Karasawa Y., Tanaka I., Miyahara J., Takahashi K., Saito H. et al. (1994) An imaging plate neutron detector. Nucl. Instrum. Methods. **A349:** 521–525
4 Haga Y. K., Kumazawa S. and Niimura N. (1999) Gamma-ray sensitivity and shielding of a neutron imaging plate. J. Appl. Cryst. **32:** 878–882
5 Haga Y. K., Neriishi K., Takahashi K. and Niimura N. (2002) Optimization of neutron imaging plate. Nucl. Instrum. Methods Phys. Research **A487:** 504–510
6 Niimura N., Minezaki Y., Nonaka T., Castagna J. C., Cipriani F., Hoghej P. et al. (1997) Neutron Laue diffractometry with an imaging plate provides an effective data collection regime for neutron protein crystallography. Nat. Struct. Biol. **4:** 909–914
7 Helliwell J. R. and Wilkinson C. (1994) X-ray and neutron Laue diffraction. In: Neutron and Synchrotron Radiation for Condensed Matter Studies: Applications to Soft Condensed Matter and Biology, chap. 7, vol. 3, Baruchel J., Hodeau J.-L., Lehmann M., Regnard J. R. and Schlenkar C. (eds.), Springer, Berlin
8 Schoenborn B. P., Saxena A. M., Stamm M., Dimmler G. and Radeka V. (1985) A neutron spectrometer with a two-dimensional detector for time-resolved studies. Australian Journal of Physics: **38:** 337–351
9 Schoenborn B. P. and Langan P. (2004) Protein crystallography with spallation neutrons. J. Synchrotron Radiat. **11:** 80–82
10 Helliwell J. R. (1997) Neutron Laue diffraction does it faster. Nat. Struct. Biol. **4:** 874–876
11 Raghavan N. V. and Woldawer A. (1987) Neutron crystallography of proteins. Methods Exp. Phys. Part C **23:** 335–365
12 Schoenborn B. P. (1985) Experimental neutron protein crystallography. Methods Enzymol. **114:** 510–529
13 Schoenborn B. P. (ed.) (1984) Neutrons in Biology, Plenum Press, New York
14 Schoenborn B. P. and Knott R. B. (eds.) (1996) Neutrons in Biology, Basic Life Sciences Series, vol. 64, Plenum Press, New York
15 Kossiakoff A. A. (1985) The application of neutron crystallography to the study of dynamic and hydration properties of proteins. Annu. Rev. Biochem. **54:** 1195–1227
16 Niimura N. (1999) Neutrons expand the field of structural biology. Curr. Opin. Struct. Biol. **9:** 602–608
17 Tsyba I. and Bau R. (2002) Neutron diffraction studies of proteins. Chemtracts **15:** 233–257
18 Niimura N., Chatake T., Ostermann A., Kurihara K. and Tanaka I. (2003) High resolution neutron protein crystallography: hydrogen and hydration in proteins. Z. Kristallogr. **218:** 96–107
19 Niimura N., Chatake T., Kurihara K. and Maeda M. (2004) Hydrogen and hydration in proteins. Cell Biochem. Biophys. **40:** 351–370
20 Meilleur F., Blakeley M. and Myles D. A. A. (2005) Neutron laue analysis of hydrogen and hydration in protein structures. In: Hydrogen- and Hydration-Sensitive Structural Biology, pp. 75–86, Niimura N., Mizuno H., Helliwell J. R. and Westhof E. (eds.), KubaPro, Tokyo
21 Blakeley M., Hazemann I., Myles D. A. A. and Podjarny A. D. (2005) Protonation states in human aldose reductase observed with high-resolution X-ray crystallography and preliminary neutron diffraction results. In: Hydrogen- and Hydration-Sensitive Structural Biology, pp. 87–102, Niimura N., Mizuno H., Helliwell J. R. and Westhof E. (eds.) KubaPro, Tokyo
22 Habash J., Raftery J., Nuttall R., Price H. J., Wilkinson C., Kalb A. J. et al. (2000) Direct determination of the positions of the deuterium atoms of the bound water in concanavalin A by neutron Laue crystallography. Acta Cryst. **D56:** 541–550
23 Myles D. A. A., Bon C., Langan P., Cipriani F., Castagna J. C., Lehmann, M. S. et al. (1998) Neutron Laue diffraction in macromolecular crystallography. Physica **B241&243:** 1122–1130
24 Langan P., Greene G. and Schoenborn B. P. (2004) Protein crystallography with spallation neutrons: the User Facility at Los Alamos Neutron Science Center. J. Appl. Cryst. **37:** 24–31
25 Langan P. and Greene G. (2004) Protein crystallography with spallation neutrons: collecting and processing wavelength-resolved Laue protein data. J. Appl. Cryst. **37:** 253–257
26 Schoenborn B. P. and Langan P. (2004) Protein crystallography with spallation neutrons. J. Synchrotron Rad. **11:** 80–82

27 Tanaka I., Kurihara K., Chatake T. and Niimura N. (2002) A high-performance neutron diffractometer for biological crystallography (BIX-3). J. Appl. Cryst. **35:** 34–40
28 Kurihara K., Tanaka I., Muslih M. R., Ostermann A. and Niimura N. (2004) A new neutron single-crystal diffractometer dedicated for biological macromolecules (BIX-4). J. Synchrotron Radiat. **11:** 68–71
29 Schultz A. J. (1993) Single-crystal time-of-flight neutron diffraction. Trans. Amer. Cryst. Assoc. **29:** 29–41
30 Wilson C. C. (1995) A guided tour of ISIS, the UK Spallation Source. Neutron News **23:** 313–316
31 Keen, D. A. and Wilson, C. C. (1996) Single Crystal Diffraction at ISIS, User guide for the SXD Instrument, Rutherford Lab Technical Report RAL-TR-96-083
32 Kurihara K., Tanaka I., Chatake T., Adams M. W., Jenney F. E. Jr., Moiseeva N. et al. (2004) Neutron crystallographic study on rubredoxin from Pyrocuccus furiosus by BIX-3, a single-crystal diffractometer for biomacromolecules. Proc. Natl. Acad. Sci. USA **101:** 11215–11220
33 Chatake T., Kurihara K., Tanaka I., Tsyba I., Bau R., Jenney F. E. et al. (2004) A neutron crystallographic analysis of a rubredoxin mutant at 1.6 Å resolution. Acta Cryst. **D60:** 1364–1373
34 Li, X., Langan, P., Bau, R., Tsyba, I., Jenny, F. E. Adams, M. W. W. and Schoenborn, B. P. (2004). A preliminary time-of-flight neutron diffraction study of the W3Y single mutant of Rubredoxin from pyrococcus furiosus. Acta Cryst. **D60:** 200–202
35 Arai S., Chatake T., Minezaki Y. and Niimura N. (2002) Crystallization of a large single crystal of a B-DNA decamer for a neutron diffraction experiment by the phase-diagram technique. Acta Cryst. **D58:** 151–153
36 Chatake T., Mizuno N., Voordouw G., Higuchi Y., Arai S., Tanaka I. et al. (2003) Crystallization and preliminary neutron analysis of the dissimilatory sulfite reductase D (DsrD) protein from the sulfate-reducing bacterium Desulfovibrio vulgaris. Acta Cryst. **D59:** 2306–2309
37 Maeda M., Chatake T., Tanaka I., Ostermann A. and Niimura N. (2004) Crystallization of a large single crystal of cubic insulin for neutron protein crystallography. J. Synchrotron Radiat. **11:** 41–44
38 Arai S., Chatake T., Suzuki N., Mizuno H. and Niimura N. (2004) More rapid evaluation of biomacromolecular crystals for diffraction experiments. Acta Cryst. **D60:** 1032–1039
39 Gamble T. R., Clauser K. R. and Kossiakoff A. A.(1994) The production and X-ray structure determination of perdeuterated Staphylococcal nuclease. Biophys. Chem. **53:** 15–25
40 Shu F., Ramakrishnan V. and Schoenborn B. P. (2000) Enhanced visibility of hydrogen atoms by neutron crystallography on fully deuterated myoglobin. Proc. Natl. Acad. Sci. USA **97:** 3872–3879
41 Langan P., Bennet B., Dealwis C., Stone D. Li X., Schoenborn B. P. et al. (2004) LANSCE Activity Report, Los Alamos National Laboratory, Los Alamos, New Mexico, USA, March 22
42 Myles D. A. A. (2004) Abstracts of the Amer. Cryst. Assoc. Meeting, Chicago, July
43 Garman E. (1999) Cool data: quantity and quality. Acta Cryst. **D55:** 1641–1653
43a Hanson B. L. (2004) Getting protein solvent structures down cold: Proc. Natl. Acad. Sci. USA **101:** 16393–16394
44 Bon C., Lehmann M. S. and Wilkinson C. (1999) Quasi-Laue neutron-diffraction study of the water arrangement in crystals of triclinic hen egg-white lysozyme. Acta Cryst. **D55:** 978–987
45 Blakeley M. P., Kalb A. J., Helliwell J. R. and Myles D. A. A. (2004) The 15-K neutron structure of saccharide-free concanavalin A. Proc. Natl. Acad. Sci. USA **101:** 16405–16410
46 Ostermann A., Tanaka I., Engler N., Niimura N. and Parak F. G. (2002) Hydrogen and deuterium in myoglobin as seen by a neutron structure determination at 1.5 Å resolution. Biohpys. Chem. **95:** 183–193
47 Maeda M., Fujiwara S., Yonezawa Y. and Niimura N. (2001) Neutron structure analysis of hen egg-white lysozyme at pH4.9. J. Phys. Soc. Jpn. Suppl. A, **70:** 403–405
48 Arai S., Chatake T., Ohhara T., Kurihara K., Tanaka I., Suzuki N. et al. (2005) Complicated water orientations in the minor groove of B-DNA decamer d(CCATTAATGG)$_2$ observed by neutron diffraction measurements. Nucleic Acids Res. **33:** 3017–3024
49 Chatake T., Tanaka I., Umino H., Arai S. and Niimura N. (2005) Neutron crystallographic analysis of the Z-DNA hexamer CGCGCG. Acta Cryst. **D61:** 1088–1098
50 Baker E. N. and Hubbard R. E. (1984) Hydrogen bonding in globular proteins. Prog. Biophys. Molec. Biol. **44:** 97–179
51 Preissner R., Egner U. and Saenger W. (1991) Occurrence of bifurcated three-center hydrogen bonds in proteins. FEBS Lett. **288:** 192–196
52 Hiller R., Zhou Z. H., Adams M. W. W. and Englander S. W. (1997) Stability and dynamics in a hyperthermophilic protein with melting temperature close to 200 °C. Proc. Natl. Acad. Sci. USA **94:** 11329–11332
53 Hernandez G., Jenney F. E. Jr., Adams M. W. W. and LeMaster D. M. (2000) Millisecond time scale conformational flexibility in a hyperthermophile protein at ambient temperature. Proc. Natl. Acad. Sci. USA **97:** 3166–3170
54 Matsuo H., Oe M., Sakiyama F. and Narita K. (1972) A new approach to the determination of pKa's of histidine residues in proteins. J. Biochem. **72:** 1057–1060
55 Brandes R. and Ehrenberg A. (1986) Kinetics of the proton-deuteron exchange at position H8 of adenine and guanine in DNA. Nucleic Acids Res. **14:** 9491–9508
56 Gursky O., Li Y., Badger J.and Casper D. L. D. (1992) Monovalent cation binding to cubic insulin crystals. Biophys. J. **61:** 604–611
57 Phillips D. C. (1966) The three-dimensional structure of an enzyme molecule. Sci. Am. **215:** 75–80
58 Mason S. A., Bentley G. A. and McIntyre G. J. (1984) Deuterium exchange in lysozyme at 1.4 Å resolution. In: Neutrons in Biology, pp. 323–334, Schoenborn B. P. (ed.), Plenum Press, New York
59 Cooper J. B. and Myles D. A. A. (2000) A preliminary neutron Laue diffraction study of the aspartic proteinase endothiapepsin. Acta Cryst. **D56:** 246–248
60 Coates L., Erskine P. T., Wood S. P., Myles D. A. A. and Cooper J. B. (2001) A neutron Laue diffraction study of endothiapepsin: implications for the aspartic proteinase mechanism. Biochemistry **40:** 13149–13157
61 Hanson B. L., Langan P., Katz A. K., Li X. M., Harp J. M., Glusker J. P. et al. (2004) A preliminary time-of-flight neutron diffraction study of Streptomyces rubiginosus D-xylose isomerase. Acta Cryst. **D60:** 241–249
62 Fenn T. D., Ringe D. and Petsko G. A. (2004) Xylose isomerase in substrate and inhibitor michaelis states: atomic resolution studies of a metal-mediated hydride shift. Biochemistry **43:** 6464–6474
63 Howard E. I., Sanishvili R., Cachau R. E., Mitschler A., Chevrier B., Barth P. et al. (2004) Ultrahigh resolution drug design: details of interactions in human aldose reductase-inhibitor complex at 0.66 Å. Proteins **55:** 792–804
64 Meilleur F. (2004) Thesis, University J. Fourier, Grenoble
65 Sukumar N., Langan P., Mathews F. S., Jones L. H., Thiyagarajan P., Schoenborn B. P. et al. (2005) A preliminary time-of-flight neutron diffraction study on amicyanin from *Paracoccus denurificans*. Acta Cryst. D: 61 (Pt 5): 640–642
66 Zhu Z., Cunane L. M., Chen Z., Durley R. C., Mathews F. S. and Davidson V. L. (1998) Molecular basis for interprotein complex-dependent effects on the redox properties of amicyanin. Biochemistry **37:** 17128–17136
67 Elgren T. E., Orville A. M., Kelly K. A., Lipscomb J. D., Ohlendorf D. H. and Que L. Jr. (1997) Crystal structure and resonance

Raman studies of protocatechuate 3,4-dioxygenase complexed with 3,4-dihydroxyphenylacetate. Biochemistry **36:** 11504–11513
68 Brown C. K., Langan P., Scoenborn B. P., Earhart C. A. and Ohlendorf D. H. (2004) Abstracts of the Amer. Cryst. Assoc. Meeting, Chicago, July
69 Daniels B. V., Myles D. A. A., Forsyth V. T. and Lawson C. L. (2003) Crystals of trp repressor suitable for high-resolution neutron Laue diffraction studies. Acta Cryst. **D59:** 136–138
70 Chatake T., Ostermann A., Kurihara K., Parak F. G. and Niimura N. (2003) Hydration in proteins observed by high-resolution neutron crystallography. Proteins **50:** 516–523
71 Wing W., Drew H., Takano T., Broka C., Tanaka S., Itakura K. et al. (1980) Crystal structure analysis of a complete turn of B-DNA. Nature **287:** 755–758
72 Tereshko V., Minasov G. and Egli M. (1999) The Dickerson-Drew B-DNA dodecamer revisited at atomic resolution. J. Am. Chem. Soc. **122:** 470–471
73 Minasov G., Tereshko V. and Egli M. (1999) Atomic-resolution crystal structures of B-DNA reveal specific influences of divalent metal ions on conformation and packing. J. Mol. Biol. **291:** 83–99
74 Goodsell D. S., Kaczor-Grzeskowiak M. and Dickerson R. E. (1994) The crystal structure of C-C-A-T-T-A-A-T-G-G. Implications for bending of B-DNA at T-A steps. J. Mol. Biol. **239:** 79–96
75 Rich A. and Zhang S. (2003) Timeline: Z-DNA: the long road to biological function. Nat. Rev. Genet. **4:** 566–572
76 Wang A. H., Quigley G. J., Kolpak F. J., Crawford J. L., van Boom J. H., van der Marel G. et al. (1979) Molecular structure of a left-handed double helical DNA fragment at atomic resolution. Nature **282:** 680–686
77 Bancroft D., Willians L. D., Rich A. and Egli M. (1994) The low-temperature crystal structure of the pure-spermine form of Z-DNA reveals binding of a spermine molecule in the minor groove. Biochemistry **33:** 1073–1086
78 Egli M., Williams L. D., Gao Q. and Rich A. (1991) Structure of the pure-spermine form of Z-DNA (magnesium free) at 1 Å resolution. Biochemistry **30:** 11388–11402
79 Gessner R. V., Quigley G. J. and Egli M. (1994) Comparative studies of high resolution Z-DNA crystal structures. Part **1:** Common hydration patterns of alternating dC-dG. J. Mol. Biol. **236:** 1154–1168
80 Habash J., Raftery J., Weisgerber S., Cassetta A., Lehmann M. S., Hoghoj P. et al. (1997) Neutron Laue diffraction study of concanavalin A: the proton of Asp-28. J. Chem. Soc. Faraday Trans. **93:** 4313–4319
81 Kalb (Gilboa) A. J., Myles D. A. A., Habash J., Raftery J. and Helliwell J. R. (2001) Neutron Laue diffraction experiments on a large unit cell: concanavalin A complexed with methyl-α-D-glucopyranoside. J. Appl. Cryst. **34:** 454–457
82 Ahmed H., Blakerly M., Habash J. and Helliwell J. R. (2005) Atomic detail structural studies on concanavalin A and extending the large molecular weight frontier of neutron protein crystallography to virus crystals. In: Hydrogen- and Hydration-Sensitive Structural Biology, pp. 63–74, Niimura N., Mizuno H., Helliwell J. R. and Westhof E. (eds.), KubaPro, Tokyo


To access this journal online:
http://www.birkhauser.ch